The Astrophysical Journal Supplement Series, 262:18 (14pp), 2022 September https://doi.org/10.3847/1538-4365/ac7deb

The Spectral Energy Distributions for 4FGL Blazars

J. H. Yang[1,2], J. H. Fan[2,3], Y. Liu[2,3], M. X. Tuo[1], Z. Y. Pei[2], W. X. Yang[2], Y. H. Yuan[2,3], S. L. He[2], S. H. Wang[1], X. C. Wang[1], X. J. Chen[1], X. H. Qu[1], Q. Cao[1], Q. Y. Tao[1], Y. L. Zhang[1], C. Q. Liu[1], J. J. Nie[1], L. F. Liu[1], D. K. Jiang[1], A. N. Jiang[1], B. Liu[1], and R. S. Yang[1]
[1] College of Mathematics and Physics Science, Hunan University of Arts and Science, Changde 415000, People's Republic of China; yjianghe@163.com
[2] Center for Astrophysics, Guangzhou University, Guangzhou 510006, People's Republic of China; fjh@gzhu.edu.cn
[3] Astronomy Science and Technology Research Laboratory of Department of Education of Guangdong Province, Guangzhou 510006, People's Republic of China
Received 2021 August 15; revised 2022 June 2; accepted 2022 June 9; published 2022 August 24

Abstract

In this paper, the multiwavelength data from radio to X-ray bands for 2709 blazars in the 4FGL-DR3 catalog are compiled to calculate their spectral energy distributions using a parabolic equation $\log(\nu f_\nu) = P_1(\log\nu - P_2)^2 + P_3$. Some important parameters including spectral curvature (P_1), synchrotron peak frequency (P_2, $\log\nu_p$), and peak luminosity ($\log L_p$) are obtained. Based on those parameters, we discussed the classification of blazars using the "Bayesian classification" and investigated some mutual correlations. We came to the following results. (1) Based on the Bayesian classification of synchrotron peak frequencies, the 2709 blazars can be classified into three subclasses, i.e., $\log(\nu_p/\mathrm{Hz}) < 13.7$ for low synchrotron peak blazars (LSPs), $13.7 < \log(\nu_p/\mathrm{Hz}) < 14.9$ for intermediate synchrotron peak blazars (ISPs), and $\log(\nu_p/\mathrm{Hz}) > 14.9$ for high synchrotron peak blazars (HSPs), and there are 820 HSPs, 750 ISPs, and 1139 LSPs. (2) The γ-ray emission has the closest relationship with radio emission, followed by optical emission, while the weakest relationship is that with X-ray emission. The γ-ray luminosity is also correlated with the synchrotron peak luminosity. (3) There are strong positive correlations between the curvature ($1/|P_1|$) and the peak frequency ($\log\nu_p$) for all subclasses (FSRQs, (high, intermediate, and low) BL Lacertae objects). For different subclasses, the correlation slopes are different, which implies that there are different acceleration mechanisms and emission processes for different subclasses of blazars.

Unified Astronomy Thesaurus concepts: Active galactic nuclei (16); Gamma-ray sources (633); Blazars (164); Quasars (1319); BL Lacertae objects (158); Spectral energy distribution (2129)

Supporting material: machine-readable table

1. Introduction

As a special subclass of active galactic nuclei (AGNs), blazars show many extreme observational properties such as highly energetic radiation, the origin of which is not very clear. They have therefore been widely studied (Yang & Fan 2010; Yang et al. 2010, 2014; Xiao et al. 2019; Pei et al. 2020a; Fraga Bernardo et al. 2021; Keenan et al. 2021; Mishra et al. 2021; Zhou et al. 2021). Blazars can be classified into BL Lacertae objects (BL Lacs) and flat spectrum radio quasars (FSRQs) by the difference of emission-line features (Ghisellini et al. 2011).

The spectral energy distribution (SED) of blazars is one of the important ways to understand the origin of their multiband emission. The whole band SED of blazars shows a bimodal structure (Urry & Padovani 1995; Fossati et al. 1998; Fan et al. 2016, 2021). The first peak (lower energy peak, also known as the synchrotron peak) is located between far-infrared and soft X-ray bands, and the second peak (higher energy peak, also known as the inverse Compton peak) is located in MeV to TeV bands (Abdo et al. 2010; Wang et al. 2018; Tuo et al. 2020), and the second peak of some BL Lacs can be well explained by a hadron model (Mannheim & Biermann 1992; Cheng & Ding 1994; Beall & Bednarek 1999). The SEDs of blazars from radio to X-ray bands were investigated by many authors (Giommi et al. 1995; Sambruna et al. 1996; Fossati et al. 1998; Nieppola et al. 2006, 2008; Abdo et al. 2010; Fan et al. 2016; Zhang & Fan 2019; Dado & Dar 2021) using different blazar samples. Then, the synchrotron peak frequencies and some related parameters are given for many blazars. However, for some blazars, the values of synchrotron peak frequency given by different literature are not completely consistent, and even are quite different for some sources. Therefore, it is necessary to find out the cause of this difference in order to give a more accurate synchrotron peak frequency.

According to the frequency of synchrotron peak, blazars were divided into three categories: low synchrotron peak (LSP) blazars, intermediate synchrotron peak (ISP) blazars, and high synchrotron peak (HSP) blazars (Abdo et al. 2010; Fan et al. 2016). The corresponding types for BL Lacs are called LBL, IBL, and HBL respectively. However, in different literature, the synchrotron peak frequency used for classification is different. For example, the classification boundary given by Nieppola et al. (2006) is 14.5 and 16.5, namely, $\log(\nu_p/\mathrm{Hz}) < 14.5$ for LSP, $14.5 < \log(\nu_p/\mathrm{Hz}) < 16.5$ for ISP, and $\log(\nu_p/\mathrm{Hz}) > 16.5$ for HSP; in a work by Abdo et al. (2010) it is 14 and 15; and in Fan et al. (2016) it is (14.0, 15.3). Padovani & Giommi (1995) first proposed dividing BL Lacs into HBL and LBL instead of radio selected BL Lacs (RBLs) and X-ray selected BL Lacs (XBLs). Most RBLs are LBLs, while most XBLs are HBLs. The dividing line between the two classes is at a ratio of $f_X/f_R \sim 10^{-11}$, where f_X and f_R are the flux densities of X-ray and radio emission respectively, and the X-ray flux is in ergs per square centimeter per second and radio flux is in jansky. Sambruna et al. (1996) classified BL Lacs into two categories, and the boundary is

Table 1
The Blazar Sample and the SEDs Fitting Results for 2709 Blazars

4FGL Name (1)	C_1 (2)	C_2 (3)	z (4)	P_1 (5)	P_2 (6)	P_3 (7)	$\log L_p$ (8)	$\log L_R$ (9)	$\log L_O$ (10)	$\log L_X$ (11)	$\log L_\gamma$ (12)	α_{RO} (13)	α_{OX} (14)
4FGL J0001.2+4741	BCU	ISP	...	−0.09	14.1	−12.54	45.05	42.83	...	...	45.07	...	...
4FGL J0001.2-0747	BLL	ISP	...	−0.12	14.1	−11.70	45.30	42.28	45.20	44.78	45.15	0.44	1.14
4FGL J0001.5+2113	FSRQ	LSP	1.11	−0.18	13.2	−11.64	46.17	42.97	45.90	45.90	46.57	0.44	1.00
4FGL J0002.4-5156	BCU	HSP	...	−0.09	15.7	−12.15	45.44	...	...	...	44.62	...	...
4FGL J0003.1-5248	BCU	HSP	...	−0.07	15.9	−12.09	45.50	...	45.42	46.03	45.27	...	0.80
4FGL J0003.3-1928	BCU	LSP	2.00	−0.13	13.3	−12.24	46.21	43.35	...	...	46.52	...	...
4FGL J0003.9-1149	BLL	LSP	0.86	−0.15	13.2	−11.64	45.90	43.07	45.46	...	45.38	0.54	...
4FGL J0004.0+0840	BLL	HSP	2.06	−0.08	15.3	−12.47	46.01	42.52	...	...	45.94	...	...
4FGL J0004.3+4614	FSRQ	LSP	1.81	−0.15	13.1	−12.41	45.93	43.12	...	45.35	46.60	...	...

Note. Column (1) is the 4FGL name. Column (2) is the classification is obtained from the 4FGL-DR3 catalog, BLL for BL Lac, FSRQ for flat spectrum radio quasar, and BCU for blazar of uncertain type. Column (3) is the classification given in the present work. $\log(\nu_p/\text{Hz}) < 13.7$ for LSP, $13.7 < \log(\nu_p/\text{Hz}) < 14.9$ for ISP, and $\log(\nu_p/\text{Hz}) > 14.9$ for HSP blazars. Column (4) is the redshift. Columns (5)–(7) are the spectral curvature (P_1), synchrotron peak frequency (P_2, $\log(\nu_p/\text{Hz})$), and peak flux (P_3, $\log(\nu_p f_{\nu_p})$) and are obtained from fitting SED respectively. Here, peak frequencies have not been corrected by redshift. Column (8) is the peak luminosity $\log(L_p/\text{erg}\cdot\text{s}^{-1})$, obtained by calculating the fitting results. Columns (9)–(12) are the luminosities of radio at 1.4 GHz ($\log L_R$), optical at 2.43×10^{14} Hz ($\log L_O$), X-ray at 1 keV ($\log L_X$), and γ-ray at 1 GeV ($\log L_\gamma$) respectively, in units of ergs per second. Columns (13) and (14) are the effective spectral index from radio 1.4 GHz to optical (2.43×10^{14} Hz), α_{RO}, and from optical (2.43×10^{14} Hz) to X-ray at 1 keV, α_{OX}, respectively.

(This table is available in its entirety in machine-readable form.)

$\log(\nu_p/\text{Hz}) = 15$, namely, it is less than 15 for LBL and more than 15 for HBL.

In this work, we will calculate the SEDs of the synchrotron emission component for a large sample of blazars from 4FGL-DR3 and discuss their classification and some other correlations. Throughout this paper, the spectral index α is defined as $f_\nu \propto \nu^{-\alpha}$.

2. Sample

In this paper, we will calculate the SEDs of synchrotron emissions for the blazars in the Fourth Fermi-LAT 12-year Source catalog (4FGL-DR3).[4] In 4FGL-DR3, there are 3743 blazars including 794 FSRQs, 1432 BL Lacs, and 1517 blazars of uncertain type (BCUs) (Abdollahi et al. 2022). The multiwavelength data from radio to X-ray are obtained from the NASA/IPAC Extragalactic Database (NED).[5] Finally, 2709 blazars with sufficient data to calculate SED are obtained. Among the 2709 blazars, two sources (4FGL J1242.4-2948, 4FGL J2055.8+1545) are not in 4FGL-DR3, and they are from 4FGL-DR2 (Abdollahi et al. 2020). The 2709 blazars and relevant data and calculation results are listed in Table 1.

3. Calculation Method and Results for SEDs

First, the observed data (flux densities) from radio to X-ray bands are compiled in the NED for each blazar in our sample. In addition, Galactic extinction correction is performed for the optical data. We consulted the source literature of X-ray data (such as Ackermann et al. 2015; Britzen et al. 2007; Collinge et al. 2005; Brinkmann et al. 1994, etc.), the soft X-ray data have been corrected by Galactic absorption. Before calculating SEDs, the multiband (radio to X-ray) flux densities were not K-corrected. Second, the plots of SEDs of $\log((\nu f_\nu)/(\text{erg cm}^{-2}\,\text{s}^{-1}))$ versus $\log(\nu/\text{Hz})$ are drawn for all sources. Third, the SEDs are fitted using a parabolic equation of $\log(\nu f_\nu) = P_1(\log\nu - P_2)^2 + P_3$, where P_1, P_2, and P_3 are constants (see also Fan et al. 2016).

[4] https://fermi.gsfc.nasa.gov/ssc/data/access/lat/
[5] http://ned.ipac.caltech.edu/

The physical meanings of the parameters P_1, P_2, and P_3 are as follows: P_1 is the spectral curvature; P_2 is the synchrotron peak frequency ($\log\nu_p$); and P_3 is the peak flux related to the peak frequency ($\log(\nu_p f_{\nu_p})$). The parameters P_1, P_2, and P_3 will be obtained by fitting the SEDs. When fitting SEDs, some points (some of the observational data) are masked and are not taken into account in fitting, because they should be caused by some features that are not related to the jet, which include some low-energy radio, infrared, "blue bump," and X-ray data, as well as some data deviating from the fitting curve. Whether or not the X-ray data come from synchrotron radiation is determined by the γ-ray radiation spectral shape. If X-ray and γ-ray data can well fit the second peak (inverse Compton peak), it is considered that X-ray is dominated by the inverse Compton process, otherwise it is dominated by the synchrotron radiation process. For low-frequency radio (generally less than 10^8 Hz), infrared, and "blue bump" data points, if those points obviously deviate from the parabola trend of all data points of the source, those points will be not included in fitting, that is, they will be masked in a color point in SED diagrams (Figure 1).

According to above method, the SEDs fitting results are given for 2709 blazars; there are 760 FSRQs, 1142 BL Lacs, and 807 BCUs. The result parameters include spectral curvature (P_1), synchrotron peak frequency (P_2, $\log\nu_p$) and peak flux (P_3, $\log(\nu_p f_{\nu_p})$). The fitting results for 2709 blazars are listed in Table 1.

4. Classification of Blazars with Synchrotron Peak Frequency

For the synchrotron peak frequency (P_2, $\log(\nu_p/\text{Hz})$) of 2709 4FGL-DR3 blazars, their distribution and Bayesian information criterion (BIC) values are shown in Figures 2(a) and (b). As in Fan et al. (2016), if the crossing points of two adjacent Gaussian curves are used as the classification boundaries, then the analysis results show that the boundary values ($\log(\nu_p/\text{Hz})$) are 13.66 and 14.91. Therefore, the boundary values of 13.7 and 14.9 are adopted to classify blazars in this paper. Adopting the acronyms of LSP, ISP, and HSP (Abdo et al. 2010), then

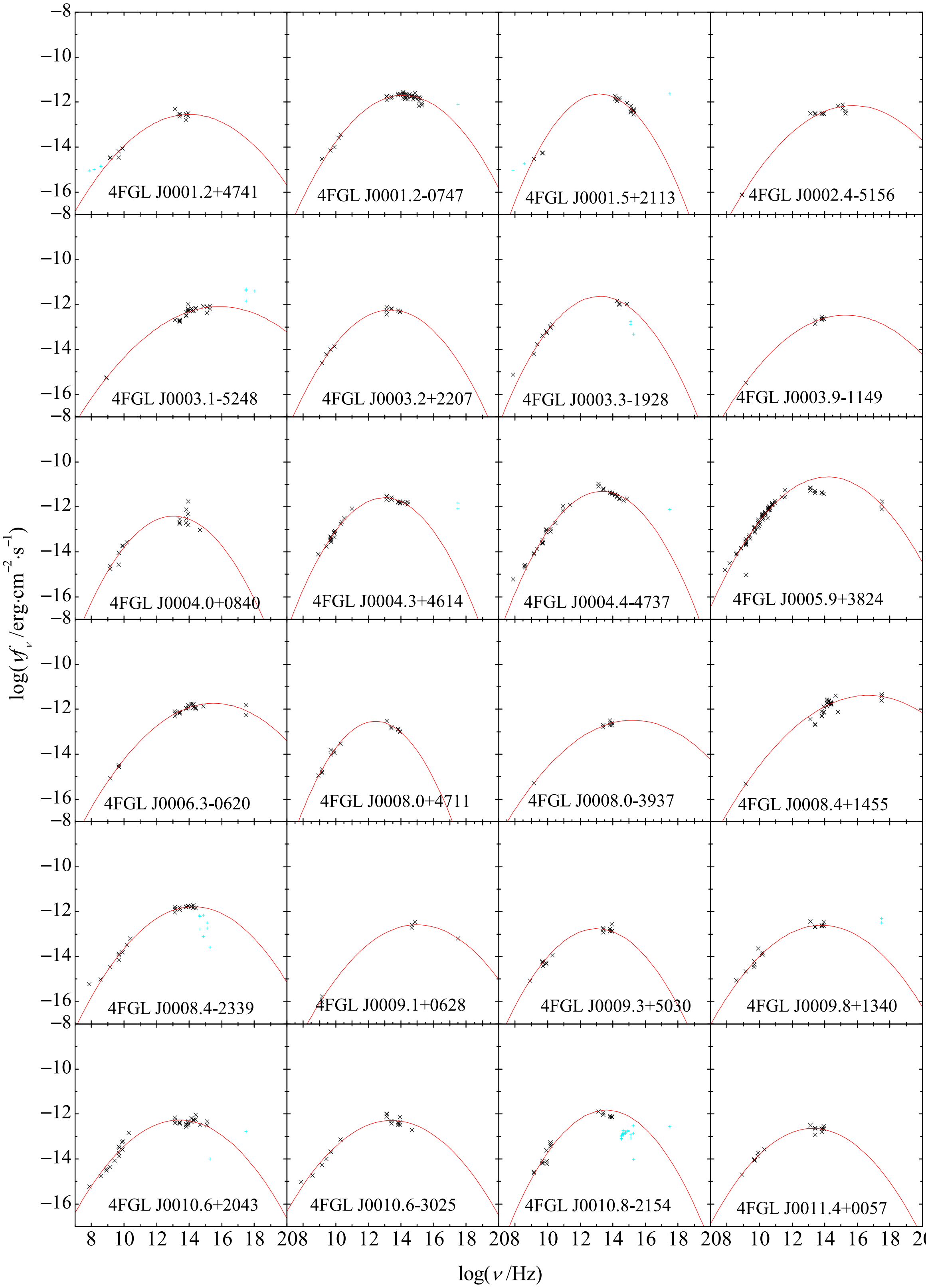

Figure 1. The SEDs diagrams with fitted lines. The curve line represents the parabolic fit to the synchrotron component. Oblique cross hairs (×) are included in the fit, the cross hairs (+) are not.

the classification criteria are $\log(\nu_{\rm p}/{\rm Hz}) < 13.7$ for LSPs, $13.7 < \log(\nu_{\rm p}/{\rm Hz}) < 14.9$ for ISPs, and $\log(\nu_{\rm p}/{\rm Hz}) > 14.9$ for HSPs. Here, peak frequencies have not been corrected by redshift. In the subsequent calculation, the synchrotron peak frequency will be corrected by redshift. The correction method is $\nu_{\rm peak}^{\rm observer\ frame} = \nu_{\rm peak}^{\rm comoving\ frame}(1 + z)$.

The results of classification are shown in Column (3) of Table 1. The histogram of types for 2709 blazars is shown in

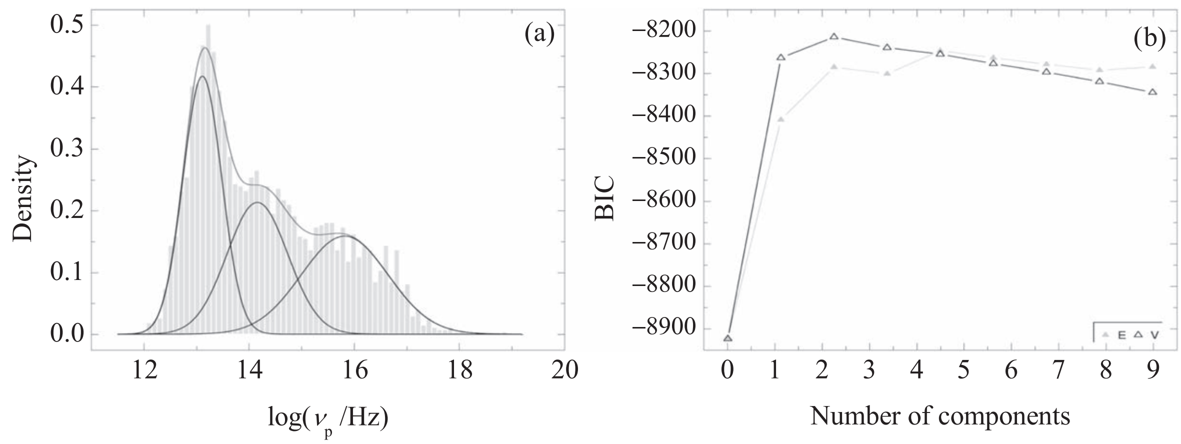

Figure 2. The BIC values and distribution for the synchrotron peak frequencies of 2709 blazars. (a) Distribution. (b) BIC values.

Figure 3, from which we can get the following results. For the 2709 blazars, 820 are HSP, accounting for 30.27%; 750 are ISP, accounting for 27.69%; 1139 are LSP, accounting for 42.05%. For the 1142 BL Lacs, 671 are HBL, accounting for 58.76%; 339 are IBL, accounting for 29.68%; 132 are LBL, accounting for 11.56%. For the 760 FSRQs, 5 are HSP, accounting for 0.66%; 124 are ISP, accounting for 16.32%; 631 are LSP, accounting for 80.03%. For the 807 BCUs, 144 are HSP, accounting for 17.84%; 287 are ISP, accounting for 35.56%; 376 are LSP, accounting for 46.59%.

Therefore, HSPs are more than LSPs in BL Lacs, while LSPs are more than HSPs in FSRQs. There are only 5 HSPs in 760 FSRQs. The proportion of HSP, ISP, and LSP in BCUs is basically the same as that in total sample.

In the sample of BL Lacs + FSRQs, BL Lacs account for 60.04%, while FSRQs account for 39.96%. "BCU" is the blazar candidate of uncertain type (Ajello et al. 2020; Abdollahi et al. 2020). If we assume that the proportion of BL Lacs and FSRQs in BCUs is similar to that in the known sample of BL Lacs + FSRQs, then we have that BL Lacs account for about 60%, while FSRQs account for about 40% in BCUs sample, namely, there are about 323 FSRQs and 484 BL Lacs in 807 BCUs. This conclusion is helpful to study the classification of BCUs (Germani et al. 2021; Fraga Bernardo et al. 2021).

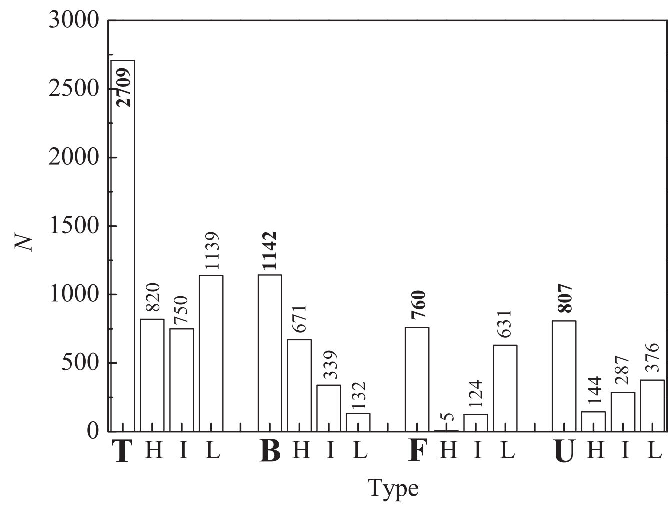

Figure 3. The distribution of classification for 2709 blazars. T stands for total sample, B for BL Lac, F for FSRQ, U for blazars of uncertain type, H for HSP, I for ISP, and L for LSP.

5. Comparison for Peak Frequencies

The SEDs of $\log(\nu f_\nu)$ versus $\log \nu$ were calculated by many authors using different samples of blazars (Sambruna et al. 1996; Fossati et al. 1998; Nieppola et al. 2006, 2008; Abdo et al. 2010; Fan et al. 2016). The synchrotron peak frequency was obtained by fitting SED using a logarithmic parabola of $\log(\nu f_\nu) = A(\log \nu)^2 + B \log \nu + C$. In this paper, we obtained 2709 SEDs and the corresponding peak frequencies of 4FGL-DR3 blazars using the same method. So, it is possible for us to compare the peak frequency of this work ($\log \nu_p^{\rm TW}$) with those of other works ($\log \nu_p^{\rm OW}$). The comparison results are shown in Figure 4 and Table 2. Figures 4(a)–(f) are the correlations between $\log \nu_p^{\rm TW}$ and $\log \nu_p^{\rm OW}$. Figures 4(a′)–(f′) are the correlations between $\log \nu_p^{\rm TW}$ and $\log(\nu_p^{\rm TW}/\nu_p^{\rm OW})$. The other works are Sambruna et al. (1996; S96; Figures 4(a), (a′)), Nieppola et al. (2006; N06; Figures 4(b), (b′)), Nieppola et al. (2008; N08; Figure 4(c), (c′)), Abdo et al. (2010; A10; Figures 4(d),(d′)), Fan et al. (2016; F16; Figures 4(e), (e′)), and Paliya et al. (2021; P21; Figures 4(f), (f′)), respectively.

Table 2 shows that there are good correlations between the results from this work and those from other works. The correlation coefficients are all more than 0.7 and the chance probabilities are all less than 10^{-4}.

For the 35 common sources of this paper and Sambruna et al. (1996), we have that the average values of the logarithm of peak frequencies are $\overline{\log \nu_p^{\rm TW}} = 14.17$ for this work and $\overline{\log \nu_p^{\rm S96}} = 14.22$ for Sambruna et al. (1996). For the 128 sources in common with Nieppola et al. (2006), there are $\overline{\log \nu_p^{\rm TW}} = 15.14$ and $\overline{\log \nu_p^{\rm N06}} = 15.41$. For the 82 sources in common with Nieppola et al. (2008), there are $\overline{\log \nu_p^{\rm TW}} = 13.41$ and $\overline{\log \nu_p^{\rm N08}} = 13.27$. For the 47 sources in common with Abdo et al. (2010), there are $\overline{\log \nu_p^{\rm TW}} = 14.03$ and $\overline{\log \nu_p^{\rm A10}} = 14.00$. For the 1276 sources in common with Fan et al. (2016), there are $\overline{\log \nu_p^{\rm TW}} = 14.45$, $\overline{\log \nu_p^{\rm F16}} = 14.40$. For the 863 sources in common with Paliya et al. (2021), there are $\overline{\log \nu_p^{\rm TW}} = 13.91$, $\overline{\log \nu_p^{\rm P21}} = 13.61$. Therefore, on the average, the results in present work are consistent with those in the

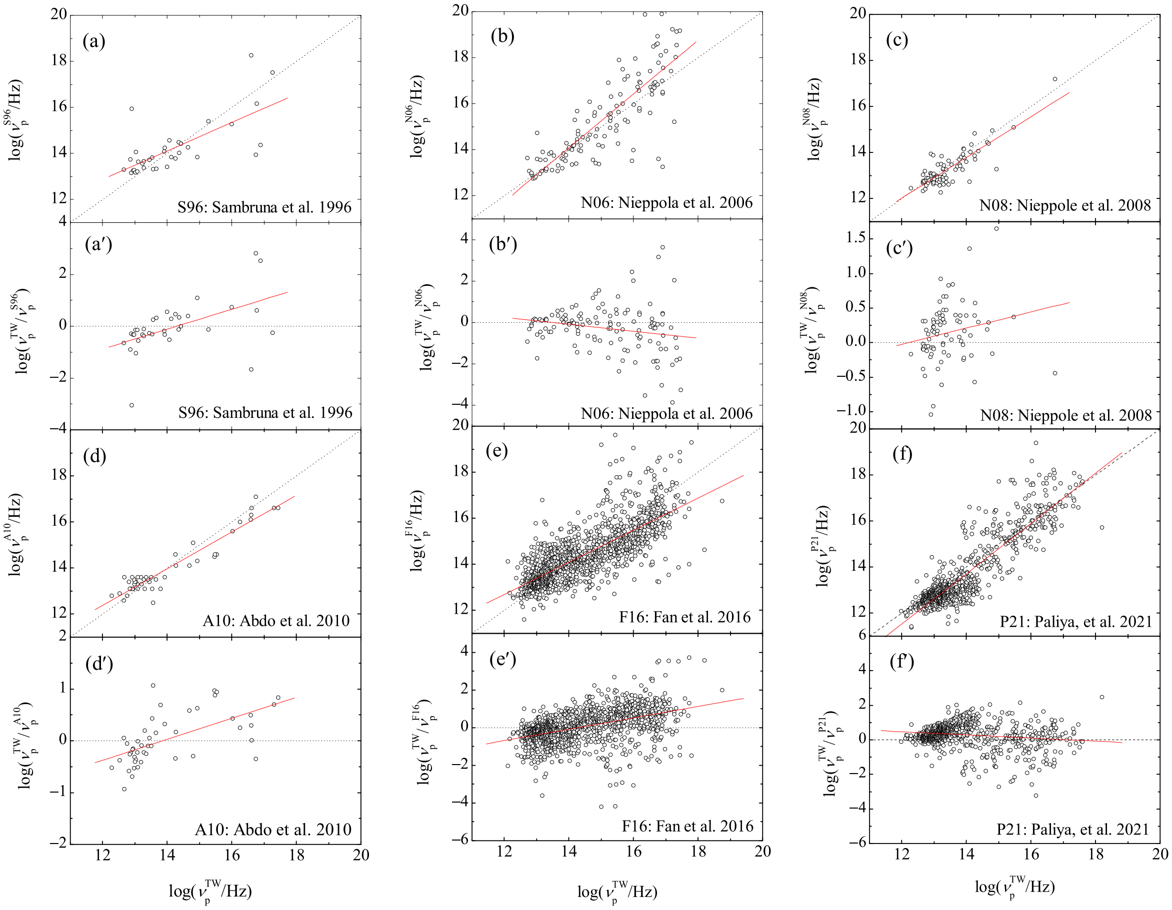

Figure 4. The correlations between the synchrotron peak frequencies obtained from this work and other works. TW: this work. S96: Sambruna et al. (1996). N06: Nieppola et al. (2006). N08: Nieppola et al. (2008). A10: Abdo et al. (2010). F16: Fan et al. (2016). P21: Paliya et al. (2021).

Table 2
The Correlations between the Synchrotron Peak Frequencies Obtained from This Work and Other Works

$y \sim x$ (1)	a (2)	Δa (3)	b (4)	Δb (5)	r (6)	n (7)	p (8)
$\log \nu_p^{S96} \sim \log \nu_p^{TW}$	5.46	1.56	0.62	0.11	0.70	35	<0.0001
$\log(\nu_p^{TW}/\nu_p^{S96}) \sim \log \nu_p^{TW}$	−5.46	1.56	0.38	0.11	0.52	35	0.0014
$\log \nu_p^{N06} \sim \log \nu_p^{TW}$	−2.27	1.08	1.17	0.07	0.83	128	<0.0001
$\log(\nu_p^{TW}/\nu_p^{06}) \sim \log \nu_p^{TW}$	2.27	1.08	−0.17	0.07	−0.21	128	0.0193
$\log \nu_p^{N08} \sim \log \nu_p^{TW}$	1.42	0.86	0.88	0.06	0.84	82	<0.0001
$\log(\nu_p^{TW}/\nu_p^{08}) \sim \log \nu_p^{TW}$	−1.42	0.86	0.12	0.06	0.20	82	0.0725
$\log \nu_p^{A10} \sim \log \nu_p^{TW}$	2.81	0.56	0.80	0.04	0.95	47	<0.0001
$\log(\nu_p^{TW}/\nu_p^{A10}) \sim \log \nu_p^{TW}$	−2.81	0.56	0.20	0.04	0.60	47	0.0011
$\log \nu_p^{F16} \sim \log \nu_p^{TW}$	4.32	0.24	0.70	0.02	0.77	1276	<0.0001
$\log(\nu_p^{TW}/\nu_p^{F16}) \sim \log \nu_p^{TW}$	−4.32	0.24	0.30	0.02	0.46	1276	<0.0001
$\log \nu_p^{F16} \sim \log \nu_p^{TW}$	−1.58	0.26	1.09	0.02	0.89	863	<0.0001
$\log(\nu_p^{TW}/\nu_p^{F16}) \sim \log \nu_p^{TW}$	1.58	0.26	−0.09	0.02	−0.17	863	0.0200

Note. In Table 2, r is the correlation coefficient, p is the chance probability, n is the sample size, and the linear regression equation is expressed as $y = (a \pm \Delta a) + (b \pm \Delta b)x$.

literature (Sambruna et al. 1996; Nieppola et al. 2006, 2008; Abdo et al. 2010; Fan et al. 2016; Paliya et al. 2021).

From the comparison between the peak frequencies obtained from this work and other works, we can see that there is a difference between them, but the difference is not obvious. For the common source samples, the average peak frequency in this work is bigger than that in Nieppola et al. (2008), Abdo et al. (2010), Fan et al. (2016), and Paliya et al. (2021), while it is smaller than that in Sambruna et al. (1996) and Nieppola et al. (2006).

It is obvious from Figure 4 that for the same source, the synchrotron peak frequencies given in different literature are different, and for some sources, the difference is large. The peak frequency is determined by the data set used to calculate the SED of one source. The main reasons for this difference are as follows.

There is a difference in the data sets used to calculate SEDs. Different databases were used by different authors; this will lead to a difference in the data set. For one source, if the amount of data changes greatly, this may lead to bigger difference in peak frequency. We compared the results from this paper with those from Fan et al. (2016). For a few common sources, there is clear difference between the peak frequencies. By comparing the SED figures obtained by this paper and that by Fan et al. (2016), it can be found that the difference in peak frequency is mainly caused by the different number of data. For example, for 4FGL J1335.3-2949 (3FGL J1335.4-2949; other name 1ES 1332-295), there are 21 data in this paper, while there are only 12 data in Fan et al. (2016) for 4FGL J1535.0 +5320 (3FGL J1534.4+5323; other name 1ES 1533+535); there are 47 data in this paper, while there are only 28 in Fan et al. (2016) for 4FGL J0746.6-4754 (3FGL J0746.6-4756; other name PMN J0746-4755); there are 28 data in this paper, while there are only 8 data in Fan et al. (2016). For some common sources with Fan et al. (2016), the present fittings are better.

Different authors have different methods of data selection. Due to the limitation of the number of data, the SEDs of some sources cannot be fitted well, so it is necessary to screen the data. Different authors have different ways to screen X-ray data. For some blazars, the soft X-rays are mainly from synchrotron emission, forming the tail of the low energy peak. The high-energy X-rays are mainly from inverse Compton emission, forming the beginning of the high energy peak (Paliya et al. 2021; Fan et al. 2016; Yang et al. 2019). Therefore, when we calculate SED, we need to screen the X-ray data, and only the X-ray produced by synchrotron emission is selected. In addition, the data set used to calculate SED is nonsimultaneous data, some of which deviate from the concentrated data. Different authors have different methods to deal with these data. These will also lead to a difference in the fitting. The choice of those data for fitting SED depends on the author's experience. Therefore, there should be some differences in the synchrotron peak frequency given in different literature. In order to obtain the accurate peak frequency for a source, there must be sufficient observations for the source.

In this paper, the peak frequency estimation method is limited in precision and the uncertainty of the parameter is large, probably by the order of 0.5 dex for the peak energy. We believe that the results obtained in this paper are not accurate synchrotron peak frequencies, but they still have an important research and reference value. There are many factors affecting the synchrotron peak frequency. For example, (1) the multi-band data from radio to X-ray are all from NED. Therefore, the data are nonsimultaneous, and the integrity of the data is not enough. (2) Not all data are generated by synchrotron radiation, and it is impossible to screen out all nonsynchrotron radiation data in SED fitting. (3) The spectral trend (SED) of synchrotron radiation is not a standard parabola. (4) All data have observation errors. (5) A blazar is a highly variable source, so its peak frequency itself is not a fixed value.

6. Correlations

Based on the fitting parameters and the calculations, we will investigate their mutual correlations. For clarity, we describe the parameters and the corresponding symbols as follows: synchrotron peak frequency, $\nu_{\rm p}$; synchrotron peak luminosity, $L_{\rm p}$; spectral curvature, P_1; 1.4 GHz radio luminosity, $L_{\rm R}$; 2.43×10^{14} Hz optical luminosity, $L_{\rm O}$; 1 keV X-ray luminosity, $L_{\rm X}$; 1 GeV γ-ray luminosity, L_γ; 1.4 GHz radio flux density, $f_{\rm R}$; 2.43×10^{14} Hz optical flux density, $f_{\rm O}$; 1 keV X-ray flux density, $f_{\rm X}$; γ-ray at 1 GeV flux density, f_γ; effective spectrum index of radio to optical, $\alpha_{\rm RO}$; and effective spectrum index of optical to X-ray, $\alpha_{\rm OX}$ respectively. The relationships of some parameters discussed in this paper are as follows: (i) $\log \nu_{\rm p}$ versus $\log L_{\rm R}$, $\log L_{\rm O}$, $\log L_{\rm X}$, $\log L_\gamma$, $\log L_{\rm p}$, $1/|P_1|$, $\alpha_{\rm RO}$, $\alpha_{\rm OX}$, respectively; (ii) $\log f_\gamma$ versus $\log f_{\rm R}$, $\log f_{\rm O}$, $\log f_{\rm X}$, respectively; (iii) $\log L_\gamma$ versus $\log L_{\rm R}$, $\log L_{\rm O}$, $\log L_{\rm X}$, $\log L_{\rm p}$ respectively. The acquisition method of those parameters for one source is as follows.

(1) P_1 *and* $\log \nu_{\rm p}$. The spectral curvature (P_1) and synchrotron peak frequency ($\log \nu_{\rm p}$) are directly obtained by fitting SED scatterplot, and the results are shown in Columns (5) and (6) of Table 1 separately. The peak frequencies in Table 1 have not been corrected by redshift. In the subsequent discussion of parameter correlation, the synchrotron peak frequencies will be corrected by the relation of $\nu_{\rm peak}^{\rm observer\ frame} = \nu_{\rm peak}^{\rm comoving\ frame}(1+z)$.

(2) $\log L_{\rm p}$, $\log L_{\rm R}$, $\log L_{\rm O}$, $\log L_{\rm X}$, *and* $\log L_\gamma$. The peak luminosity ($L_{\rm p}$) can be calculated from peak flux ($\log(\nu_{\rm p} f_{\nu_{\rm p}})$ i.e., P_3). All luminosities are calculated with the formula $L_\nu = 4\pi d_L^2 \nu f_\nu$; here, d_L is a luminosity distance (Pedro & Priyamvada 2007), $d_L = (1+z) \cdot \frac{c}{H_0} \cdot \int_1^{1+z} \frac{1}{\sqrt{\Omega_{\rm M} x^3 + 1 - \Omega_{\rm M}}} dx$.

In this work, the frequencies in radio, optical, X-ray, and γ-ray bands are chosen as $\nu_{\rm R} = 1.4$ GHz, $\nu_{\rm O} = 2.43 \times 10^{14}$ Hz, $\nu_{\rm X} = 2.42 \times 10^{17}$ Hz (1 keV), and $\nu_\gamma = 2.42 \times 10^{23}$ Hz (1 GeV) respectively. The flux density, $f_{\rm R}$, $f_{\rm O}$, and $f_{\rm X}$, were collected from the data set used to calculate SED. If a source has more than one data at a certain frequency ($\nu_{\rm R}$, $\nu_{\rm O}$, and $\nu_{\rm X}$), we will select the data with a smaller error and being close to the median value. The flux densities obtained from NED will be K-corrected with the formula $f_\nu = f_\nu^{\rm ob}(1+z)^{(\alpha_\nu - 1)}$; here α_ν is a spectral index at frequency ν, and z is redshift. In the K-correction of flux densities and the luminosities calculation, if the redshift (z) or the spectral index (α_ν) for one source is not available, the average value of the same type source is adopted (Donato et al. 2001; Fan et al. 2016).

According to the above method, the luminosities including $L_{\rm p}$, $L_{\rm R}$, $L_{\rm O}$, $L_{\rm X}$, and L_γ are calculated, and the results are listed in Columns (8)–(12) of Table 1.

(3) $\alpha_{\rm RO}$ *and* $\alpha_{\rm OX}$. The effective spectrum index from frequency ν_1 to frequency ν_2 is defined (Ledden & Odell 1985; Fan et al. 2012; Yang et al. 2018; Nie et al. 2020) as $\alpha_{12} = -\frac{\log(f_1/f_2)}{\log(\nu_1/\nu_2)}$, where f_1 and f_2 are the flux densities at ν_1 and ν_2 respectively. The effective spectral indices calculated in this paper are radio 1.4 GHz to optical 2.43×10^{14} Hz ($\alpha_{\rm RO}$) and 2.43×10^{14} Hz to X-ray 1 keV ($\alpha_{\rm OX}$). The calculative results of effective spectral indices are listed in Columns (13) and (14) of Table 1, respectively.

Although the statistical results of IBL and BCU have been shown in this paper, we will not consider them in the discussion of parameter correlations below, because IBL is the intermediate state between HBL and LBL, while BCU is an unknown type of blazar, and their statistical significance is not obvious.

6.1. The Correlations between Peak Frequencies and Other Parameters

The diagrams of the relationships between $\log \nu_{\rm p}$ and other parameters are shown in Figure 5, and the linear fitting results are listed in Table 3. In Table 3, r is a correlation coefficient, p is the chance probability, n is the sample size, and the linear regression relation is expressed as $y = (a \pm \Delta a) + (b \pm \Delta b)x$.

(1) *Monochromatic luminosity* $\log L_{\rm R}$, $\log L_{\rm O}$, $\log L_{\rm X}$, *and* $\log L_{\gamma}$ *versus* $\log \nu_{\rm p}$ *(Figures 5(a)–(d) and Table 3)*. For $\log L_{\rm R}$ versus $\log \nu_{\rm p}$ (Figure 5(a)), there are strong anticorrelations for the whole sample and the subsamples of FSRQs and BL Lacs (HBLs and LBLs). It is obtained that $\log L_{\rm R} = -(0.60 \pm 0.01)\log \nu_{\rm p} + (50.83 \pm 0.20)$ with a correlation coefficient $r = -0.67$ and chance probability $p < 10^{-4}$ for the whole sample. For $\log L_{\rm O}$ versus $\log \nu_{\rm p}$, a weak anticorrelation can be found for all samples (Figure 5(b)). For $\log L_{\rm X}$ versus $\log \nu_{\rm p}$, there are different correlations for the whole sample and subsamples, positive correlations for BL Lacs and the subsample of HBLs, anticorrelation for FSRQs and LBLs (Figure 5(c)). For $\log L_{\gamma}$ versus $\log \nu_{\rm p}$ (Figure 5(d)), there is a good anticorrelation between them, and $\log L_{\gamma} = -(0.47 \pm 0.01)\log \nu_{\rm p} + (51.84 \pm 0.20)$ with $r = -0.54$ and $p < 10^{-4}$ for the whole sample. Anticorrelations are also found for the subclasses. All the corresponding results are listed in Table 3 for details.

Nieppola et al. (2008) indicated that the strong anticorrelation between $\log L_{\rm R}$ (or $\log L_{\gamma}$) and $\log \nu_{\rm p}$ may be due to a beaming effect. We know that the Doppler factor (δ) is larger for lowly peaked sources than that for highly peaked sources. A larger δ results in a larger boosting, while a smaller δ results in a weaker boosting. In addition, the γ-ray and radio emissions are all strongly beamed, which will also lead to an anticorrelation between $\log L_{\rm R}$ (or $\log L_{\gamma}$) and $\log \nu_{\rm p}$.

Between $\log L_{\rm O}$ and $\log \nu_{\rm p}$, a weak anticorrelation is shown for all samples. In optical bands, there may be different radiation mechanisms from low energy to high energy. In addition, there are the host galaxy emissions for BL Lacs and accretion for FSRQs. Therefore, the correlation between $\log L_{\rm O}$ and $\log \nu_{\rm p}$ will be diluted by those effects.

In X-ray bands, the emissions are located at the tail of synchrotron radiation and the beginning of an inverse Compton radiation (Fan et al. 2016; Yang et al. 2019; Paliya et al. 2021). The X-ray emissions are mainly from synchrotron radiation for HBLs, which will result in a positive correlation between $\log L_{\rm X}$ and $\log \nu_{\rm p}$. However, for FSRQs and LBLs, the X-ray emissions are mainly from inverse Compton radiation, and the lower the synchrotron peak frequency is, the more the contribution from inverse Compton radiation in the X-ray band is, so it will result in an anticorrelation between $\log L_{\rm X}$ and $\log \nu_{\rm p}$.

In this paper, we use the average value to replace the redshift of the sources without redshift. It may affect the true relationship between luminosity and peak frequency, especially for the BL Lacs sample. In order to know the magnitude of this effect, we recalculated the relationship between luminosity and peak frequency using the sample of only BL Lacs with redshift; the results are shown in Table 4. For the convenience of comparison, the results of correlation between luminosity and peak frequency for all BL Lacs samples are also listed in Table 4. From Table 4, it is obvious that the sample size of the sample of only BL Lacs with redshift is significantly smaller than that of whole BL Lacs. But, the results in Table 4 show that there is no obvious difference between two results obtained from two samples. Therefore, the average redshift of the same type blazars is used for the source without redshift, which has little effect on the correlation between luminosity and peak frequency.

(2) $\log L_{\rm p}$ *versus* $\log \nu_{\rm p}$ *(Figure 5(e) and Table 3)*. For $\log L_{\rm p}$ versus $\log \nu_{\rm p}$ (Figure 5 (e)), there is an anticorrelation for samples of whole ($r = -0.25$, $p < 10^{-4}$) and FSRQs ($r = -0.35$, $p < 10^{-4}$), but no correlation is found for BL Lacs ($r = 0.00$, $p = 96.49\%$). When the subclasses of BL Lacs are considered separately, there is a weak positive correlation for HBLs ($r = 0.11$, $p = 0.63\%$), and an anticorrelation for LBLs ($r = -0.30$, $p = 0.05\%$).

For the whole sample, we have a clear anticorrelation between $\log L_{\rm p}$ and $\log \nu_{\rm p}$ implying that sources become brighter with the decreasing peak frequency. When we consider FSRQs and BL Lacs separately, an anticorrelation still exists for FSRQs, but there is no correlation for BL Lacs. The reason is that there is different dependence of peak frequency luminosity on the peak frequency; there is a positive correlation for HBLs while there is an anticorrelation for LBLs, and there is no correlation for IBLs. Therefore, there is almost no correlation for the whole BL Lacs. The positive correlation for HBLs is consistent with the discovery that higher peak frequency BL Lacs have higher luminosity (Giommi et al. 1995). Fossati et al. (1998) showed that $\log \nu_{\rm p}$ decreased with the increase of luminosity. But for XBLs, this phenomenon is not obvious. The results of the present paper consistent with those of Fossati et al. (1998). Nieppola et al. (2008) also studied the correlation between $\log L_{\rm p}$ and $\log \nu_{\rm p}$ of blazars samples, and found that there was an intrinsic positive correlation between them. Also, they found that the Doppler factor decreases with the increase of peak frequency, so the source with high peak frequency may have weak beaming effect. Therefore, the anticorrelation between $\log L_{\rm p}$ and $\log \nu_{\rm p}$ may be caused by the beaming effect. Since Doppler boosting decreases with peak frequency, the Doppler factor of the source with higher peak frequency is smaller (Nieppola et al. 2008; Yang et al. 2022). Therefore, HBL has weak Doppler boosting (Pei et al. 2020b; Yang et al. 2012). While for FSRQs and LBLs, the anticorrelation between $\log L_{\rm p}$ and $\log \nu_{\rm p}$ is from their Doppler factors. In 2017, Fan et al. (2017) investigated the correlation between luminosity and peak frequency for observed data and intrinsic data. The anticorrelation for the observed data became positive correlation for the intrinsic data. Our present results are consistent with those by Fossati et al. (1998), Nieppola et al. (2006, 2008), and Fan et al. (2016). But the apparent anticorrelation may be from the beaming effect or selection effect.

(3) $1/|P_1|$ *versus* $\log \nu_{\rm p}$ *(Figure 5(f) and Table 3)*. It is found that $1/|P_1| = (1.97 \pm 0.03)\log \nu_{\rm p} - (18.58 \pm 0.39)$, with $r = 0.81$ and $p < 10^{-4}$ for the whole sample. The detailed correlations for other samples are shown in Table 3. In the work by Fan et al. (2016), the correlation between peak frequency ($\log \nu_{\rm p}$) and logarithm spectral curvature ($\log|P_1|$) was discussed, and a good correlation between them was found. Chen (2014) discussed the correlation between synchrotron peak frequency and curvature in detail using the spectral curvature obtained from a Fermi bright blazars sample.

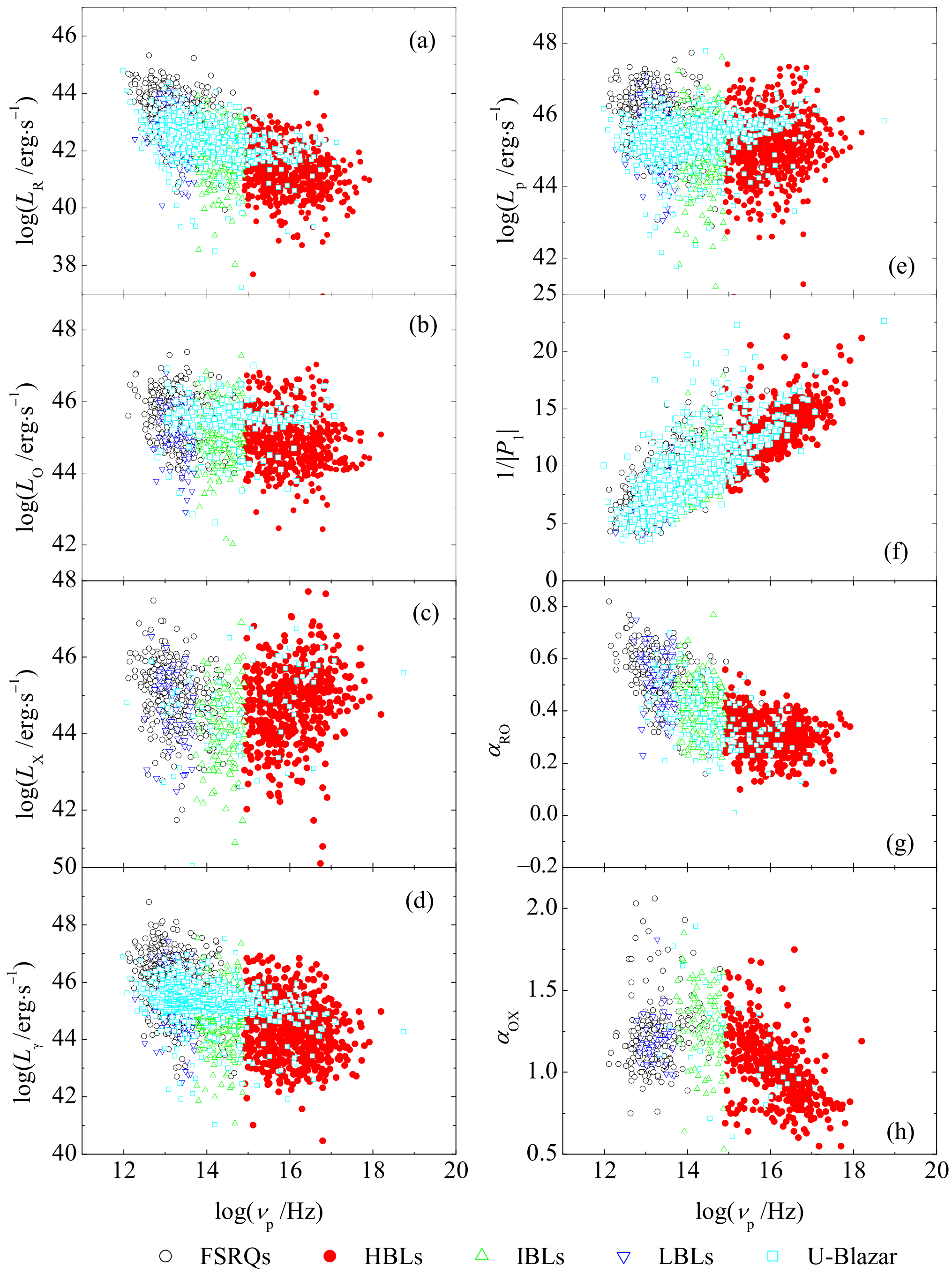

Figure 5. The scatterplots of the correlations between $\log \nu_{\mathrm{p}}$ and other parameters of (a) $\log L_{\mathrm{R}}$, (b) $\log L_{\mathrm{O}}$, (c) $\log L_{\mathrm{X}}$, (d) $\log L_{\gamma}$, (e) $\log L_{\mathrm{p}}$, (f) $1/|P_1|$, (g) α_{RO}, and (h) α_{OX}.

He found that there is a statistically significant correlation between them. Therefore, our results are consistent with those by Fan et al. (2016) and Chen (2014).

The X-ray spectra of some sources (e.g., MRK 421, MRK 501) obey the logarithmic parabola rule, and there is a strong correlation between the peak frequency and curvature (Massaro et al. 2004, 2006; Tramacere et al. 2007, 2009). Tramacere et al. (2007, 2009, 2011) pointed out that the strong correlation between the peak frequency and curvature in the SED of synchrotron radiation is caused by the random component in the acceleration process. We have used the logarithmic parabola, $\log(\nu f_{\nu}) = P_1(\log \nu_{\mathrm{p}} - P_2)^2 + P_3$, to fit the SED of the synchrotron emission for 2709 blazars. It is found that there is a strong correlation between the peak frequency (ν_{p}) and the curvature ($1/|P_1|$). This strong correlation is in favor of the random acceleration probability of particles. Chen (2014) explained the observed correlation between synchrotron peak frequency and curvature in the SED of synchrotron radiation. If the relation is $1/|P_1| = A + B \cdot \log \nu_{\mathrm{p}}$, Chen (2014) proposed some theoretical predictions of the slope B, namely $B = 5/2$, $10/3$, and 2 are for models of energy dependent acceleration probability, fluctuation of fractional acceleration gain, and stochastic acceleration, respectively. Our linear fitting result (Table 3) gives $B_{\mathrm{Total}} = 1.97 \pm 0.03$ for total sample,

Table 3
The Linear Fitting Results of the Correlations between $\log \nu_p$ and Other Parameters

$y \sim x$ (1)	Sample (2)	a (3)	Δa (4)	b (5)	Δb (6)	r (7)	n (8)	p (9)
$\log L_R \sim \log \nu_p$	T	50.83	0.20	−0.60	0.01	−0.67	2265	<0.0001
	F	51.61	0.66	−0.63	0.05	−0.44	676	<0.0001
	B	47.79	0.37	−0.41	0.02	−0.48	965	<0.0001
	H	46.44	0.85	−0.33	0.05	−0.25	558	<0.0001
	I	47.07	2.40	−0.37	0.17	−0.13	289	0.0292
	L	56.32	3.28	−1.04	0.25	−0.37	118	<0.0001
	U	46.69	0.40	−0.31	0.03	−0.40	624	<0.0001
$\log L_O \sim \log \nu_p$	T	47.93	0.23	−0.19	0.02	−0.31	1442	<0.0001
	F	50.86	0.92	−0.40	0.07	−0.30	333	<0.0001
	B	46.26	0.34	−0.09	0.02	−0.13	882	0.0001
	H	46.39	0.79	−0.10	0.05	−0.08	541	0.0543
	I	44.97	1.95	0.00	0.14	0.00	254	0.9786
	L	55.05	3.89	−0.75	0.29	−0.27	87	0.0119
	U	45.28	0.63	0.01	0.04	0.02	227	0.7890
$\log L_X \sim \log \nu_p$	T	45.45	0.28	−0.04	0.02	−0.07	1192	0.0199
	F	51.57	0.88	−0.49	0.07	−0.33	450	<0.0001
	B	41.80	0.52	0.18	0.03	0.21	670	<0.0001
	H	39.66	1.03	0.32	0.06	0.22	490	<0.0001
	I	37.73	4.07	0.45	0.28	0.14	126	0.1134
	L	54.78	5.64	−0.76	0.43	−0.24	54	0.0806
	U	39.90	1.60	0.32	0.11	0.34	72	0.0039
$\log L_\gamma \sim \log \nu_p$	T	51.84	0.20	−0.47	0.01	−0.54	2708	<0.0001
	F	54.08	0.80	−0.61	0.06	−0.35	760	<0.0001
	B	48.91	0.39	−0.29	0.03	−0.32	1141	<0.0001
	H	48.43	0.92	−0.26	0.06	−0.17	671	<0.0001
	I	46.16	2.31	−0.10	0.16	−0.03	338	0.5479
	L	55.68	3.51	−0.79	0.26	−0.25	132	0.0034
	U	48.53	0.34	−0.23	0.02	−0.32	807	<0.0001
$\log L_p \sim \log \nu_p$	T	47.65	0.18	−0.16	0.01	−0.25	2708	<0.0001
	F	51.83	0.58	−0.45	0.04	−0.35	760	<0.0001
	B	45.03	0.35	0.00	0.02	0.00	1141	0.9649
	H	42.82	0.81	0.14	0.05	0.11	671	0.0063
	I	46.20	2.14	−0.08	0.15	−0.03	338	0.5695
	L	56.20	3.08	−0.83	0.23	−0.30	132	0.0005
	U	43.89	0.31	0.10	0.02	0.16	807	<0.0001
$1/\lvert P_1\rvert \sim \log \nu_p$	T	−18.58	0.39	1.97	0.03	0.81	2708	<0.0001
	F	−30.14	1.49	2.86	0.11	0.68	760	<0.0001
	B	−21.56	0.59	2.14	0.04	0.85	1141	<0.0001
	H	−22.30	1.39	2.19	0.09	0.70	671	<0.0001
	I	−28.34	3.75	2.62	0.26	0.48	338	<0.0001
	L	−23.80	5.06	2.32	0.38	0.47	132	<0.0001
	U	−21.69	1.03	2.21	0.07	0.73	807	<0.0001
$\alpha_{RO} \sim \log \nu_p$	T	1.52	0.03	−0.08	0.00	−0.73	1218	<0.0001
	F	1.61	0.13	−0.08	0.01	−0.43	299	<0.0001
	B	1.31	0.04	−0.06	0.00	−0.65	744	<0.0001
	H	0.78	0.08	−0.03	0.01	−0.27	449	<0.0001
	I	1.30	0.28	−0.06	0.02	−0.22	217	0.0013
	L	1.83	0.59	−0.10	0.04	−0.25	78	0.0281
	U	1.28	0.11	−0.06	0.01	−0.52	175	<0.0001
$\alpha_{OX} \sim \log \nu_p$	T	2.31	0.07	−0.08	0.00	−0.49	845	<0.0001
	F	0.47	0.32	0.06	0.02	0.15	253	0.0205
	B	2.88	0.11	−0.12	0.01	−0.56	557	<0.0001
	H	3.67	0.20	−0.16	0.01	−0.54	404	<0.0001
	I	3.88	0.91	−0.18	0.06	−0.27	109	0.0052
	L	1.15	1.12	0.00	0.08	0.01	44	0.9723
	U	3.51	0.66	−0.15	0.04	−0.52	35	0.0012
$\alpha_{RO} \sim \alpha_{OX}$	T	0.24	0.03	0.15	0.02	0.24	738	<0.0001
	F	0.75	0.04	−0.16	0.03	−0.35	228	<0.0001
	B	0.21	0.02	0.12	0.02	0.25	482	<0.0001
	H	0.30	0.02	−0.01	0.02	−0.02	340	0.7743
	I	0.34	0.05	0.05	0.04	0.11	101	0.2637
	L	0.72	0.11	−0.15	0.09	−0.25	41	0.1129

Table 3
(Continued)

$y \sim x$ (1)	Sample (2)	a (3)	Δa (4)	b (5)	Δb (6)	r (7)	n (8)	p (9)
	U	0.29	0.08	0.03	0.06	0.08	28	0.6683
$\log f_\gamma \sim \log f_{\rm R}$	T	−11.92	0.02	0.46	0.01	0.57	2265	<0.0001
	F	−11.87	0.03	0.42	0.04	0.38	676	<0.0001
	B	−11.88	0.03	0.49	0.02	0.60	965	<0.0001
	H	−11.87	0.05	0.50	0.03	0.54	558	<0.0001
	I	−11.90	0.05	0.46	0.04	0.56	289	<0.0001
	L	−11.90	0.06	0.44	0.07	0.50	118	<0.0001
	U	−12.29	0.04	0.24	0.03	0.35	624	<0.0001
$\log f_\gamma \sim \log f_{\rm O}$	T	−11.29	0.10	0.35	0.03	0.28	1442	<0.0001
	F	−11.38	0.25	0.21	0.08	0.15	333	0.0072
	B	−10.95	0.11	0.49	0.03	0.43	882	<0.0001
	H	−10.67	0.13	0.62	0.04	0.53	541	<0.0001
	I	−10.76	0.16	0.50	0.05	0.54	254	<0.0001
	L	−11.00	0.44	0.33	0.13	0.26	87	0.0139
	U	−12.15	0.21	0.15	0.06	0.15	227	0.0251
$\log f_\gamma \sim \log f_{\rm X}$	T	−13.18	0.17	−0.13	0.03	−0.14	1192	<0.0001
	F	−11.43	0.34	0.09	0.05	0.08	450	0.0809
	B	−12.43	0.22	0.01	0.03	0.02	670	0.6976
	H	−11.26	0.25	0.23	0.04	0.25	490	<0.0001
	I	−10.51	0.57	0.25	0.08	0.26	126	0.0030
	L	−9.81	0.95	0.32	0.14	0.30	54	0.0269
	U	−13.43	0.51	−0.11	0.07	−0.17	72	0.1548

$B_{\rm BLL} = 2.14 \pm 0.04$ for BL Lacs, $B_{\rm FSRQ} = 2.86 \pm 0.11$ for FSRQs, and $B_{\rm BCU} = 2.21 \pm 0.07$ for BCUs. When the subclasses of BL Lacs are considered, it is found that $B_{\rm HBL} = 2.19 \pm 0.09$ for HBLs, $B_{\rm IBL} = 2.62 \pm 0.26$ for IBLs, and $B_{\rm LBL} = 2.32 \pm 0.38$ for LBLs. Therefore, the correlation slopes (B) are different for different subsamples. According to the proposal by Chen (2014), the different correlation slopes (B) imply that there are different acceleration mechanisms and emission processes for different subclasses of blazars.

(4) *$\alpha_{\rm RO}$ and $\alpha_{\rm OX}$ versus $\log \nu_{\rm p}$ (Figures 5(g), (h) and Table 3).* Figure 5(g) and Table 3 show good anticorrelations between $\alpha_{\rm RO}$ and $\log \nu_{\rm p}$ for the whole sample ($r = -0.73$, $p < 10^{-4}$) and all subsamples of FSRQs ($r = -0.43$, $p < 10^{-4}$), BL Lacs ($r = -0.65$, $p < 10^{-4}$), HBLs ($r = -0.27$, $p < 10^{-4}$), and LBLs ($r = -0.25$, $p = 2.81\%$). For $\alpha_{\rm OX}$ versus $\log \nu_{\rm p}$, Figure 5(h) and Table 3 show that there are anticorrelations for the whole sample ($r = -0.49$, $p < 10^{-4}$), BL Lacs ($r = -0.56$, $p < 10^{-4}$), and HBLs ($r = -0.54$, $p < 10^{-4}$), while there is a weak positive correlation for FSRQs ($r = 0.15$, $p = 0.25\%$) and no correlation found for LBLs ($r = 0.01$, $p = 97.23\%$). See Table 3 for details.

Fossati et al. (1998) discussed the correlation between $\alpha_{\rm RO}$ and $\log \nu_{\rm p}$, and found that there is an anticorrelation between them for the whole sample, with which our result is consistent. Fan et al. (2016) also discussed the correlations between $\alpha_{\rm RO}$ and $\log \nu_{\rm p}$ and between $\alpha_{\rm OX}$ and $\log \nu_{\rm p}$. In their results, except that the correlation between $\alpha_{\rm RO}$ and $\log \nu_{\rm p}$ for HBLs is inconsistent with the results of this paper, other results are consistent. Our result shows that there is an anticorrelation between $\alpha_{\rm RO}$ and $\log \nu_{\rm p}$ for HBLs with $r = -0.27$ and $p < 10^{-4}$, while no correlation is found in the paper by Fan et al. (2016) with $r = 0.07$ and $p = 48.15\%$.

For the correlation between $\alpha_{\rm RO}$ and $\log \nu_{\rm p}$, when the peak frequency increases, both radio and optical emission come from synchrotron radiation, and they will decrease, but the decrease of radio emission is larger than that of optical emission, which will lead to the decrease of $\alpha_{\rm RO}$. Therefore, there is an anticorrelation between $\alpha_{\rm RO}$ and $\log \nu_{\rm p}$.

For the correlation between $\alpha_{\rm OX}$ and $\log \nu_{\rm p}$, when the peak frequency becomes higher for the sources with higher peak frequency, the X-ray emission will increase and the optical emission will decrease, which will lead to the decrease of $\alpha_{\rm OX}$. Therefore, there is an anticorrelation between $\alpha_{\rm OX}$ and $\log \nu_{\rm p}$ for the sources with higher peak frequency, such as HBLs. However, when the peak frequency of the low peak frequency source becomes lower, the optical emission will become weaker, but the X-ray is dominated by inverse Compton, which will lead to the decrease of $\alpha_{\rm OX}$. Therefore, there is a positive correlation between $\alpha_{\rm OX}$ and $\log \nu_{\rm p}$ for the sources with lower peak frequency, such as LBLs and most FSRQs.

6.2. The Correlation between α_{RO} and α_{OX}

For $\alpha_{\rm RO}$ versus $\alpha_{\rm OX}$ (Figure 6 and Table 3), there are positive correlations for the whole sample ($r = 0.24$, $p < 10^{-4}$) and BL Lacs ($r = 0.25$, $p < 10^{-4}$). There are anticorrelations for FSRQs ($r = -0.35$, $p < 10^{-4}$) and LBLs ($r = -0.25$, $p = 11.29\%$), while no correlation is found for HBLs ($r = -0.02$, $p = 77.43\%$) (see Table 3 for details).

Figure 6 shows clearly that HBLs and FSRQs/LBLs occupy different regions in the panel, with IBLs being the bridge between them. The relation of $\alpha_{\rm RO}$ versus $\alpha_{\rm OX}$ in the present work is consistent with those reported in the literature (Padovani & Giommi 1995; Nieppola et al. 2006; Fan et al. 2016; Abdo et al. 2010; Ackermann et al. 2011).

The frequencies used for the calculation of the effective spectral indexes are $\nu_{\rm R} = 1.4$ GHz, $\nu_{\rm O} = 2.43 \times 10^{14}$ Hz, and $\nu_{\rm X} = 1$ keV in this paper, while those in Ackermann et al. (2011) are $\nu_{\rm R} = 5$ GHz, $\nu_{\rm O} = 5000$ Å, and $\nu_{\rm X} = 1$ keV. Although there are different frequencies for calculating the

Table 4
The Result of the Correlations between Luminosities (y: $\log L_{\rm R}$, $\log L_{\rm O}$, $\log L_{\rm X}$, $\log L_{\gamma}$) and Synchrotron Peak Frequency (x: $\log \nu_{\rm p}$) for the Sample of Whole BL Lacs and Only BL Lacs with Redshift

		Whole BL Lacs							BL Lacs with Redshift						
y	C	a	Δa	b	Δb	r	n	p	a	Δa	b	Δb	r	n	p
$\log L_{\rm R}$	BLL	47.79	0.37	−0.41	0.02	−0.48	965	<0.0001	48.28	0.45	−0.45	0.03	−0.48	746	<0.0001
	HBL	46.44	0.85	−0.33	0.05	−0.25	558	<0.0001	46.65	1.03	−0.35	0.06	−0.25	436	<0.0001
	LBL	56.32	3.28	−1.04	0.25	−0.37	118	<0.0001	61.17	4.25	−1.40	0.32	−0.43	88	<0.0001
$\log L_{\rm O}$	BLL	46.29	0.33	−0.09	0.02	−0.14	881	<0.0001	46.74	0.42	−0.12	0.03	−0.17	672	<0.0001
	HBL	46.82	0.74	−0.12	0.05	−0.11	540	0.0091	47.27	0.92	−0.16	0.06	−0.13	414	0.0069
	LBL	55.05	3.89	−0.75	0.29	−0.27	87	0.0119	57.73	4.95	−0.95	0.37	−0.31	65	0.0128
$\log L_{\rm X}$	BLL	41.80	0.52	0.18	0.03	0.21	670	<0.0001	42.29	0.59	0.15	0.04	0.16	547	1.52×10^{-04}
	HBL	39.66	1.03	0.32	0.06	0.22	490	<0.0001	39.58	1.21	0.31	0.08	0.21	392	<0.0001
	LBL	54.78	5.64	−0.76	0.43	−0.24	54	0.0806	55.42	5.99	−0.81	0.45	−0.25	51	0.08027
$\log L_{\gamma}$	BLL	48.93	0.38	−0.29	0.02	−0.32	1140	<0.0001	49.39	0.49	−0.32	0.03	−0.33	842	<0.0001
	HBL	48.80	0.90	−0.28	0.06	−0.19	670	<0.0001	48.79	1.13	−0.29	0.07	−0.18	500	<0.0001
	LBL	55.68	3.51	−0.79	0.26	−0.25	132	0.0034	58.13	4.79	−0.97	0.36	−0.27	95	0.0083

effective spectral indexes, we can still compare the effective spectral index ($\alpha_{\rm RO}$ or $\alpha_{\rm OX}$) obtained from this paper with those from Ackermann et al. (2011), and the comparison results are shown in Figure 7.

The linear fitting results show that there are good correlations between $\alpha_{\rm RO}^{\rm TW}$ and $\alpha_{\rm RO}^{\rm A11}$ and between $\alpha_{\rm OX}^{\rm TW}$ and $\alpha_{\rm OX}^{\rm A11}$ for all samples. There are $\alpha_{\rm RO}^{\rm A11} = (1.19 \pm 0.04)\alpha_{\rm RO}^{\rm TW} + (0.03 \pm 0.01)$ with $r = 0.81$ and $p < 10^{-4}$, and $\alpha_{\rm OX}^{\rm A11} = (0.61 \pm 0.05)\alpha_{\rm OX}^{\rm TW} + (0.57 \pm 0.05)$ with $r = 0.52$ and $p < 10^{-4}$ for the whole sample. In the $\alpha_{\rm RO}$ relationship, it is interesting that FSRQs is obviously located at the upper right hand region of the panel, while HBLs are obviously located at the lower left hand region of the panel in Figure 7(a), which can be used to distinguish between FSRQs and HBLs. In the $\alpha_{\rm OX}$ relationship, different samples are not obviously separated.

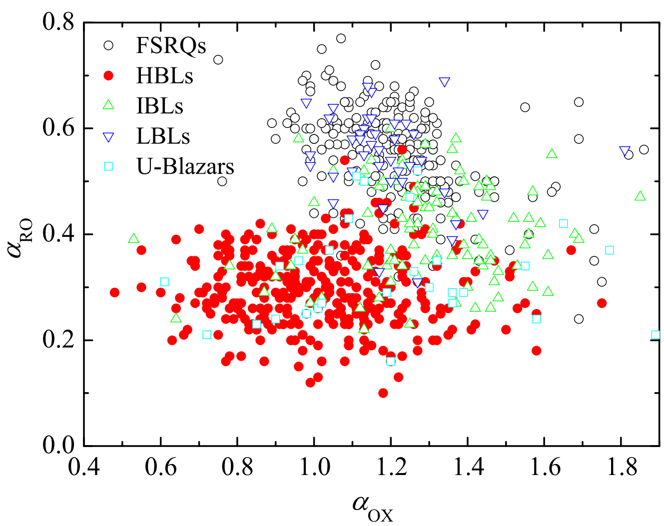

Figure 6. The correlation between $\alpha_{\rm RO}$ and $\alpha_{\rm OX}$.

6.3. The Correlations between γ-Ray Luminosity and Other Luminosity.

Now, by revisiting the correlations between γ-ray luminosity ($\log L_{\gamma}$) and radio, optical, X-ray and synchrotron peak luminosity ($\log L_{\rm R}$, $\log L_{\rm O}$, $\log L_{\rm X}$ and $\log L_{\rm p}$; see Figure 8), we found strong positive correlations between $\log L_{\gamma}$ and $\log L_{\rm R}$ ($\log L_{\rm O}$, $\log L_{\rm X}$, and $\log L_{\rm p}$), and listed the results in Table 5.

It is known that the luminosities ($\log L_{\gamma}$, $\log L_{\rm R}$, $\log L_{\rm O}$, $\log L_{\rm X}$, and $\log L_{\rm p}$) are strongly related to the redshift (z). Therefore, the correlations between $\log L_{\gamma}$ and $\log L_{\rm other}$ will be affected by redshift (Padovani 1992; Kendall & Stuart 1979) and we should remove the impact of redshift on the correlations. When the impact of redshift is removed using the method by Padovani (1992) and Kendall & Stuart (1979), the results of those correlations between luminosities are listed in Columns (10) and (11) of Table 5. It is clear that there are still good positive correlations between $\log L_{\gamma}$ and other luminosities after removing the redshift impact. Please see Columns (10) and (11) of Table 5 for details.

In this paper, the correlations between γ-ray flux density and radio (optical and X-ray) flux densities are also obtained from the same sample and the results are shown in Figure 9 and listed in Table 3.

For all samples (whole blazars, FSRQs, BL Lacs, HBLs, and LBLs), Table 3 shows that there are good positive correlations between γ-ray and radio flux density ($\log f_{\gamma}$ versus $\log f_{\rm R}$; Figure 9(a)), and also positive correlations between γ-ray and optical flux density ($\log f_{\gamma}$ versus $\log f_{\rm O}$; Figure 9(b)), but the former correlation is stronger than that of the latter. About $\log f_{\gamma}$ versus $\log f_{\rm X}$ (Figure 9(c)), there is a positive correlation for HBLs and LBLs, and a positive trend correlation for FSRQs, while there is no correlation for BL Lacs (see Table 3 for details). Therefore, for the correlation between γ-ray flux density and radio, optical, and X-ray flux density respectively, in general, the correlation between γ-ray flux density and radio flux density is the strongest, slightly weaker with optical, and the weakest with X-ray.

It is not difficult to find from Table 5 that the correlation between γ-ray luminosity and radio, optical, and X-ray luminosity is similar to that between their flux density. In other words, the correlation between γ-ray and radio is the strongest, followed by that with optical and the weakest with X-ray.

In order to further understand the high-energy γ-ray radiation mechanism of blazar, the correlations between γ-ray single frequency emission and lower energy bands emission has been studied by many authors (Fan & Wu 2018; Nieppola et al. 2011; Yang & Fan 2005; Zhang & Fan 2018; Tuo et al. 2020 and references therein). However, due to the limitation of

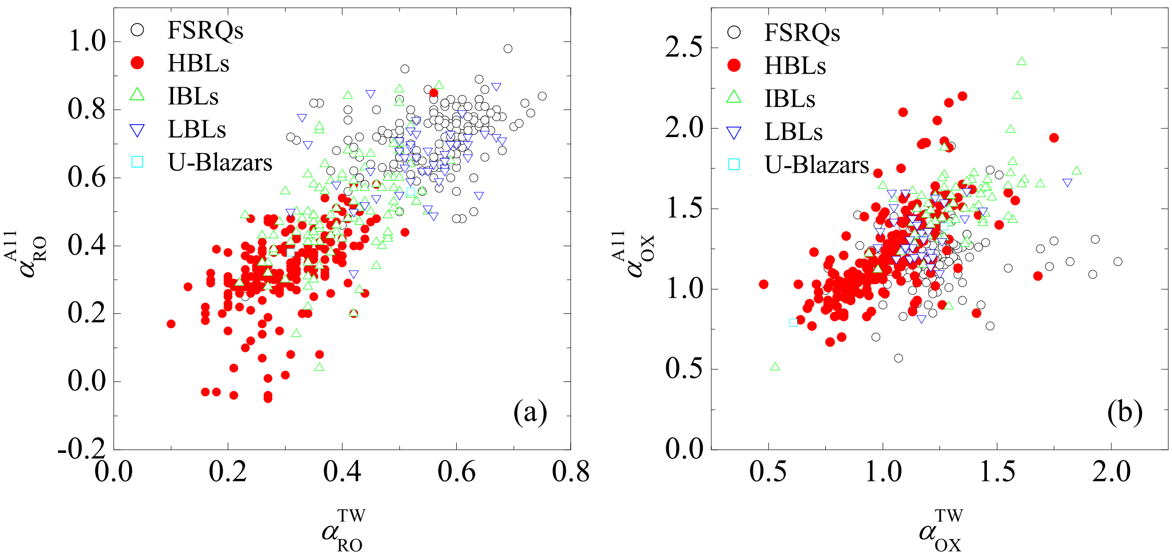

Figure 7. The correlations between effective spectral indexes obtained from this paper and Ackermann et al. (2011) (a) for α_{RO} and (b) for α_{OX}.

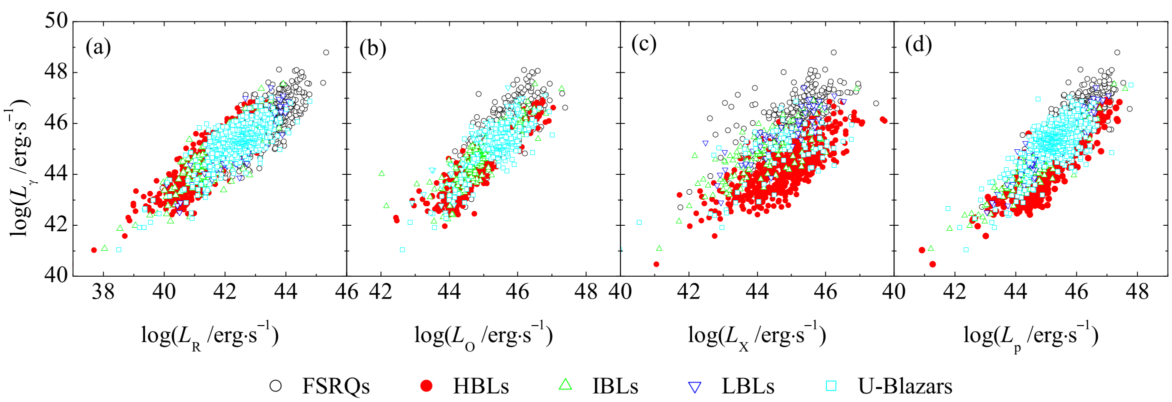

Figure 8. The correlations between two luminosities: (a) $\log L_\gamma$ and $\log L_R$, (b) $\log L_\gamma$ and $\log L_O$, (c) $\log L_\gamma$ and $\log L_X$, and (d) $\log L_\gamma$ and $\log L_p$.

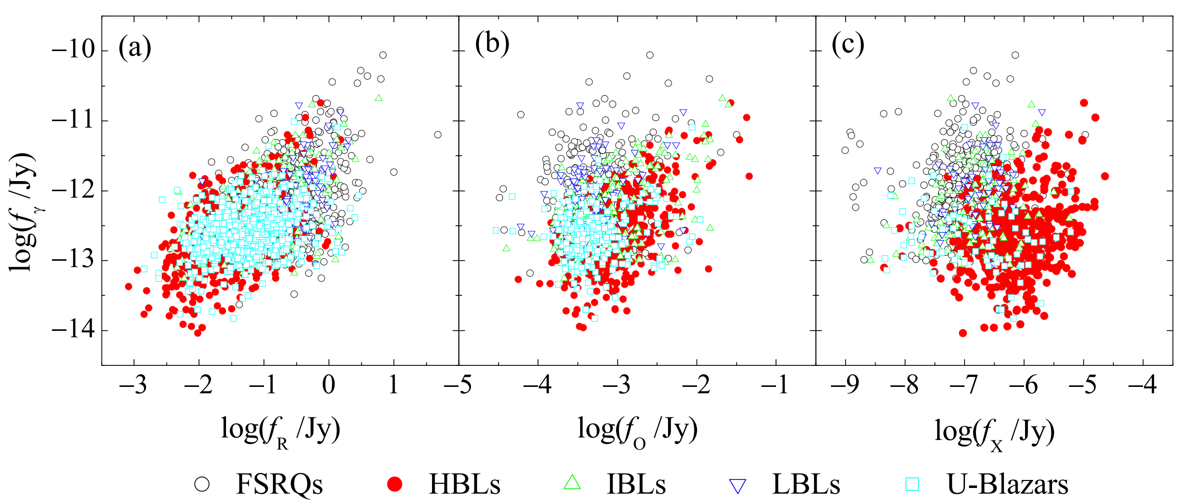

Figure 9. The correlations between flux densities: (a) $\log f_\gamma \sim \log f_R$; (b) $\log f_\gamma \sim \log f_O$; (c) $\log f_\gamma \sim \log f_X$.

sample size and accuracy of observation equipment, the results are not completely consistent. In general, the γ-ray emissions are related to radio, optical, and X-ray emissions, and also the correlation between γ-ray and radio is the strongest, followed by that with optical and the weakest with X-ray. Our results are consistent with those. In blazars, the radio and γ-ray emission are all strongly beamed (Fan et al. 2014). The strong correlation between radio and γ-ray emission may be caused by the beaming effect or the γ-ray emissions are mainly produced by the SSC process, and radio emissions from the synchrotron

Table 5
The Correlations between γ-Ray Luminosity and Other Luminosities

$y \sim x$ (1)	Sample (2)	a (3)	Δa (4)	b (5)	Δb (6)	r (7)	n (8)	p (9)	$r_{LL,z}$ (10)	$p_{LL,z}$ (11)
$\log L_\gamma \sim \log L_{\rm R}$	T	8.73	0.42	0.86	0.01	0.88	2265	<0.0001	0.47	<0.0001
	F	4.81	1.25	0.95	0.03	0.79	676	<0.0001	0.40	<0.0001
	B	7.10	0.71	0.90	0.02	0.86	965	<0.0001	0.56	<0.0001
	H	3.33	1.03	1.00	0.03	0.86	558	<0.0001	0.50	<0.0001
	I	6.53	1.34	0.91	0.03	0.86	289	<0.0001	0.51	<0.0001
	L	6.90	2.30	0.90	0.05	0.84	118	<0.0001	0.44	<0.0002
	U	12.96	1.12	0.76	0.03	0.76	624	<0.0001	0.05	0.3453
$\log L_\gamma \sim \log L_{\rm O}$	T	−11.64	0.85	1.25	0.02	0.87	1442	<0.0001	0.34	<0.0001
	F	−9.07	2.27	1.20	0.05	0.80	333	<0.0001	0.33	0.0010
	B	−9.08	0.98	1.19	0.02	0.88	882	<0.0001	0.49	<0.0001
	H	−8.82	1.05	1.18	0.02	0.91	541	<0.0001	0.59	<0.0001
	I	−4.60	1.85	1.10	0.04	0.86	254	<0.0001	0.56	<0.0002
	L	−9.69	3.28	1.22	0.07	0.88	87	<0.0001	0.39	0.0022
	U	−6.86	2.37	1.14	0.05	0.83	227	<0.0001	0.05	0.5877
$\log L_\gamma \sim \log L_{\rm X}$	T	7.04	1.33	0.85	0.03	0.64	1192	<0.0001	0.12	0.0080
	F	7.14	2.04	0.86	0.05	0.67	450	<0.0001	0.15	0.0015
	B	13.77	1.37	0.69	0.03	0.65	670	<0.0001	0.10	0.0206
	H	10.26	1.32	0.76	0.03	0.76	490	<0.0001	0.15	0.0063
	I	11.50	2.46	0.75	0.06	0.77	126	<0.0001	0.05	0.3124
	L	8.08	3.50	0.84	0.08	0.83	54	<0.0001	0.19	0.1798
	U	17.80	3.69	0.60	0.08	0.66	72	<0.0001	0.02	0.9337
$\log L_\gamma \sim \log L_{\rm p}$	T	−5.17	0.61	1.11	0.01	0.85	2708	<0.0001	0.26	<0.0001
	F	−6.03	1.28	1.13	0.03	0.83	760	<0.0001	0.53	<0.0001
	B	−1.35	0.77	1.02	0.02	0.87	1141	<0.0001	0.44	<0.0001
	H	−1.29	0.94	1.01	0.02	0.88	671	<0.0001	0.49	<0.0001
	I	−0.77	0.93	1.01	0.02	0.94	338	<0.0001	0.71	<0.0001
	L	−0.96	1.86	1.02	0.04	0.91	132	<0.0001	0.60	<0.0002
	U	9.44	1.30	0.79	0.03	0.70	807	<0.0001	0.01	0.8416

process, which will lead to a strong positive correlation between γ-ray and radio emission, or the strong positive correlation between radio and γ-ray, which maybe implies that γ-ray emission is produced cospatially with the radio emission in the jet (Nieppola et al. 2011).

7. Conclusions

Based on 4FGL-DR3 catalog, the multiwavelength data from radio to X-ray are compiled for a sample including 2709 blazars (1142 BL Lacs, 760 FSRQs, and 807 BCUs). All of the multiwavelength data are obtained from NED and used to calculate the SEDs by $\log(\nu f_\nu) = P_1(\log\nu - P_2)^2 + P_3$. The parameters including spectral curvature (P_1), synchrotron peak frequency (P_2, $\log\nu_{\rm p}$), peak flux (P_3), and peak luminosity ($\log L_{\rm p}$) are obtained, and the monochromatic luminosity and the effective spectral indexes are calculated. The results are analyzed and the correlations between some parameters are discussed. Our main conclusions are as follows.

1. The SEDs are obtained for 2709 4FGL-DR3 blazars, and the parameters including spectral curvature, synchrotron peak frequency, peak flux, and peak luminosity are given.
2. The results of "Bayesian classification" for 2709 synchrotron peak frequencies show that 2709 blazars can be classified into three subclasses. The boundary values of synchrotron peak frequency are $\log(\nu_{\rm p}/{\rm Hz}) =$ 13.7 and 14.9, i.e., $\log(\nu_{\rm p}/{\rm Hz}) < 13.7$ for LSPs, $13.7 < \log(\nu_{\rm p}/{\rm Hz}) < 14.9$ for ISPs, and $\log(\nu_{\rm p}/{\rm Hz}) >$ 14.9 for HSPs. According to this method, there are 820 HSPs, 750 ISPs, and 1139 LSPs in 2709 blazars.
3. For the 1517 BCUs in 4FGL-DR3, if we assumed BL Lacs accounted for about 60%, and FSRQs accounted for 40% as the known FSRQs and BL Lacs, then we can expect that there are about 910 BL Lacs and 607 FSRQs. The results are helpful to study the classification of BCUs.
4. The γ-ray emission is most closely related with radio emission, followed by that with optical emission, and that with X-ray emission is the weakest. The γ-ray luminosity is also correlated with synchrotron peak luminosity. This phenomenon may come from beaming effect, and implies that both γ-ray and radio emissions are strongly beamed. The lower energy radiation is mainly produced by synchrotron emission, while the high-energy γ-ray mainly comes from synchrotron self-Compton emission.
5. There are strong correlations between the curvature $(1/|P_1|)$ and the peak frequency ($\log\nu_{\rm p}$) for all subsamples. For different subsamples, the correlation slopes are different. It implies that there are different acceleration mechanisms and emission processes for different subclasses of blazars.

The work is partially supported by the National Natural Science Foundation of China (NSFC U2031112, NSFC U2031201, NSFC 11733001), Guangdong Major Project of Basic and Applied Basic Research (grant No. 2019B030302001). We also acknowledge the science research grants from the China Manned Space Project with NO. CMS-CSST-2021-A06, and the supports for Astrophysics Key Subjects of Guangdong Province and Guangzhou

City. The work is also supported by Guangzhou University (YM2020001).

This research has made use of the NASA/IPAC Extragalactic Database (NED), which is operated by the California Institute of Technology, under contract with the National Aeronautics and Space Administration. We express our sincere thanks to them!

ORCID iDs

J. H. Yang https://orcid.org/0000-0002-4469-9672
J. H. Fan https://orcid.org/0000-0002-5929-0968

References

Abdo, A. A., Ackermann, M., Agudo, I., et al. 2010, ApJ, 716, 30
Abdollahi, S., Acero, F., Ackermann, M., et al. 2020, ApJS, 247, 33
Abdollahi, S., Acero, F., Baldini, L., et al. 2022, ApJS, 260, 53
Ackermann, M., Ajello, M., Allafort, A., et al. 2011, ApJ, 743, 171
Ackermann, M., Ajello, M., Atwood, W. B., et al. 2015, ApJ, 810, 14
Ajello, M., Angioni, R., Axelsson, M., et al. 2020, ApJ, 892, 105
Beall, J. H., & Bednarek, W. 1999, ApJ, 510, 188
Brinkmann, W., Siebert, J., & Boller, Th. 1994, A&A, 281, 355
Britzen, S., Brinkmann, W., Campbell, R. M., et al. 2007, A&A, 476, 759
Chen, L. 2014, ApJ, 788, 179
Cheng, K. S., & Ding, W. K. Y. 1994, A&A, 288, 97
Collinge, M. J., Strauss, M. A., Hall, P. B., et al. 2005, AJ, 129, 2542
Dado, S., & Dar, A. 2021, ApJL, 911, L10
Donato, D., Ghisellini, G., Tagliaferri, G., & Fossati, G. 2001, A&A, 375, 739
Fan, J. H., Bastieri, D., Yang, J. H., et al. 2014, RAA, 14, 1135
Fan, J. H., Kurtanidze, S. O., Liu, Y., et al. 2021, ApJS, 253, 10
Fan, J. H., Yang, J. H., Liu, Y., et al. 2016, ApJS, 226, 20
Fan, J. H., Yang, J. H., & Xiao, H. B. 2017, ApJL, 835, L38
Fan, J. H., Yang, J. H., Yuan, Y. H., Wang, J., & Gao, Y. 2012, ApJ, 761, 125
Fan, X. L., & Wu, Q. W. 2018, ApJ, 869, 133
Fossati, G., Maraschi, L., Celotti, A., et al. 1998, MNRAS, 299, 433
Fraga Bernardo, M. O., Barres de Almeida, U., Bom, C. R., et al. 2021, MNRAS, 505, 1268
Germani, S., Tosti, G., Lubrano, P., et al. 2021, MNRAS, 505, 5853
Ghisellini, G., Tavecchio, F., Foschini, L., et al. 2011, MNRAS, 414, 2674
Giommi, P., Ansari, S. G., & Micol, A. 1995, A&AS, 109, 267
Keenan, M., Meyer, E. T., Georganopoulos, M., et al. 2021, MNRAS, 505, 4726
Kendall, M., & Stuart, A. 1979, The Advanced Theory of Statistics, Vol. 2: Inference and Relationship (4th ed.; London: Griffin)
Ledden, J. E., & Odell, S. L. 1985, ApJ, 298, 630
Mannheim, K., & Biermann, P. L. 1992, A&A, 253, L21
Massaro, E., Perri, M., Giommi, P., & Nesci, R. 2004, A&A, 413, 489
Massaro, E., Tramacere, A., Perri, M., Giommi, P., & Tosti, G. 2006, A&A, 448, 861
Mishra, H. D., Dai, X. Y., Chen, P., et al. 2021, ApJ, 913, 146
Nie, J. J., Chen, Y., Fan, J. H., et al. 2020, AcASn, 61, 9
Nieppola, E., Tornikoski, M., & Valtaoja, E. 2006, A&A, 445, 441
Nieppola, E., Tornikoski, M., Valtaoja, E., et al. 2011, A&A, 535, 69
Nieppola, E., Valtaoja, E., Tornikoski, M., et al. 2008, A&A, 488, 867
Padovani, P. 1992, A&A, 256, 399
Padovani, P., & Giommi, P. 1995, ApJ, 444, 567
Paliya, V. S., Domínguez, A., Ajello, M., et al. 2021, ApJS, 253, 46
Pedro, R. C., & Priyamvada, N. 2007, NJPh, 9, 445
Pei, Z. Y., Fan, J. H., Yang, J. H., et al. 2020a, PASP, 132, 114102
Pei, Z. Y., Fan, J. H., Yang, J. H., et al. 2020b, PASA, 37, e043
Sambruna, R. M., Maraschi, L., & Urry, C. M. 1996, ApJ, 463, 444
Tramacere, A., Massaro, F., & Cavaliere, A. 2007, A&A, 466, 521
Tramacere, A., Giommi, P., Perri, M., Verrecchia, F., & Tosti, G. 2009, A&A, 501, 879
Tramacere, A., Massaro, E., & Taylor, A. M. 2011, ApJ, 739, 66
Tuo, M. X., Deng, J. J., Yang, J. H., et al. 2020, AcASn, 61, 23
Urry, C. M., & Padovani, P. 1995, PASP, 107, 803
Wang, X. P., Bi, X. W., & Zheng, Y. G. 2018, ChA&A, 42, 360
Xiao, H. B., Fan, J. H., Yang, J. H., et al. 2019, SCPMA, 62, 129811
Yang, J. H., & Fan, J. H. 2005, ChJAA, 5, 229
Yang, J. H., Fan, J. H., & Yang, R. S. 2010, SCPMA, 53, 1162
Yang, J. H., & Fan, J. H. 2010, SCPMA, 53, 1921
Yang, J. H., Fan, J. H., & Yuan, Y. H. 2012, SCPMA, 55, 1510
Yang, J. H., Fan, J. H., Hua, T. X., et al. 2014, Ap&SS, 352, 819
Yang, J. H., Fan, J. H., Liu, Y., et al. 2018, SCPMA, 61, 059511
Yang, J. H., Fan, J. H., Zhang, Y. L., et al. 2019, AcASn, 59, 38
Yang, W. X., Wang, H. G., Liu, Y., et al. 2022, ApJ, 925, 120
Zhang, L. X., & Fan, J. H. 2018, Ap&SS, 363, 142
Zhang, Y. T., & Fan, J. H. 2019, AcASn, 60, 7
Zhou, R. X., Zheng, Y. G., Zhu, K. R., et al. 2021, ApJ, 915, 59